RSC Advances

PAPER

View Article Online
View Journal | View Issue

Cite this: *RSC Adv.*, 2019, **9**, 16106

Comparative study of hydroxyapatite, fluor-hydroxyapatite and Si-substituted hydroxyapatite nanoparticles on osteogenic, osteoclastic and antibacterial ability

Jing Sun,[a] Tao Wu,[a] Qihang Fan,[a] Qing Hu[a] and Bin Shi *[ab]

This study compared the effects of hydroxyapatite (HA), fluor-hydroxyapatite (FHA) and Si-substituted hydroxyapatite (SiHA) on osteogenic differentiation, osteoclastic activity and antibacterial properties. HA, FHA and SiHA were prepared *via* a sol–gel reaction and characterized by scanning electron microscopic analysis (SEM), transmission electron microscopic analysis (TEM), and X-ray photoelectron spectrometry. Cell proliferation was evaluated using an MTT assay and cytoskeletal morphology was observed by fluorescence microscopy. Osteogenic differentiation was evaluated using alkaline phosphatase activity and Alizarin red staining. Quantitative real-time PCR was used to evaluate the mRNA expression of runt-related transcription factor 2 (Runx2) and osteopontin (OPN). New bone formation was tested using μCT, haematoxylin and eosin staining and TRAP staining. The antibacterial actions against *Porphyromonas gingivalis* (P. g) were evaluated through plate counting and live-dead bacterial staining. The results demonstrated that HA, FHA and SiHA can promote proliferation of bone mesenchymal stem cells (BMSCs). ALP activity in FHA extract with a concentration of 625 μg mL^{-1} was the highest after 14 days osteogenic induction; similar results were observed for Runx2 and OPN mRNA expression. HA, FHA and SiHA decreased trabecular space in bone defects, but FHA reduced osteoclastic activity and inhibited P. g growth. In conclusion, FHA can promote osteogenic activity, reduce osteoclastic activity and enhance antibacterial effects.

Received 31st January 2019
Accepted 21st March 2019

DOI: 10.1039/c9ra00839j

rsc.li/rsc-advances

Introduction

There are nearly 2.2 million patients worldwide who are going to receive bone grafting to repair bone defects resulting from trauma, infection, tumour resection or osteoradionecrosis before undergoing oral implant surgery.[1] Bone augmentation is a surgical procedure that involves the repair of defective bone with a biological or synthetic bone graft. However, the source of the autologous bone graft is limited and necessitates secondary surgical incision. The development of synthetic bone substitutes is considered as being important in overcoming the intrinsic limitations of biological bone grafts.

Hydroxyapatite [HA, $Ca_{10}(PO_4)_6(OH)_2$] is one of the most important inorganic minerals in biological hard tissue and nearly 60–70% of bone tissue is composed of HA.[2,3] HA is also considered to be a suitable synthetic bone substitute or implant coating material owing to its biocompatibility and osteoconductivity.[4–6] However, there remain several disadvantages of HA as a bone substitute. The mismatch of HA degradation rate and the new bone formation rate imposes restrictions on its' use.[7] Meanwhile, as an implant coating material, the relatively high solubility results in the detachment of the coating layer, leading to implantation failure.[8–11] However, HA in natural bone can be combined with other ions such as Mg^{2+}, Zn^{2+}, Sr^{2+}, Ag^{+}, Si^{4+} and F^{-}[12,13] to promote bone remodelling and tissue regeneration, impart magnetic properties, add antibacterial activity, enhance bio-integration, *etc.*

Fluoridated hydroxyapatite [FHA, $Ca_{10}(PO_4)_6(OH)_{2-x}F_x$], is an inorganic substance in which a fluorine ion (F^{-}) replaces the hydroxyl group (OH)in HA. Fluorine (F) is an important constituent of bone and teeth. An appropriate concentration of F (a fluoridation degree of 0.8–1.1 (the x value in $Ca_{10}(PO_4)_6(OH)_{2-x}F_x$)) can promote the proliferation of the osteoblasts[14–17] and accelerate new bone formation.[7,18] Fluoride can promote osteoblast activity, which may be related to the Ras-Raf-MAPK mitogenic signal transduction pathway[19,20] and the Wnt/β-catenin signalling pathway.[21] F can also inhibit bacterial growth and protect teeth from caries.[22,23] In addition, FHA possesses better chemistry and heat stability, better mechanical strength, better biocompatibility and a longer biodegradation period[23–26] compared to HA.

[a]*The State Key Laboratory Breeding Base of Basic Science of Stomatology (Hubei-MOST), Key Laboratory of Oral Biomedicine Ministry of Education, School & Hospital of Stomatology, Wuhan University, Wuhan, 430079, CN, China. E-mail: shibin_dentist@whu.edu.cn*

[b]*Department of Dental Implantology, School and Hospital of Stomatology, Wuhan University, China*

Silicon-substituted hydroxyapatite [SiHA, $Ca_{10}(PO_4)_{6-x}(SiO_4)_x(OH)_2$] is an inorganic material with silicate (SiO_4) substituting for phosphate (PO_4) in HA. Silicon (Si) is another essential trace element involved in bone formation and calcification.[27–29] Si^{4+} can promote calcification along with Ca^{2+} and enforce the attachment, proliferation and osteogenic differentiation of bone mesenchymal stem cells (BMSCs).[27,30,31] Moreover, SiHA shows better osteoconductivity and osteoblast proliferation abilities than HA.[32,33] It has been reported that osteoblasts on 0.8 wt% SiHA have the best bioactivity.[34,35] With its structure a faster biodegradation rate, which matches the natural bone formation rate better than HA.[34]

Even though many studies have reported the physicochemical properties and biological characteristics of HA, FHA and SiHA, no studies to date have compared the effects of the three materials on bone formation *in vitro* and *in vivo* with reference to their use as a bone substitute. Therefore, the aim of this study was to systematically investigate the effects of HA, FHA and SiHA nanoparticles on cell proliferation, bone formation or resorption and antibacterial abilities *in vitro* and *in vivo*.

Material and methods

HA preparation

HA nanoparticles were prepared *via* sol–gel method by dropping an $(NH_4)_2HPO_4$ aqueous solution into a stirred $Ca(NO_3)_2$ aqueous solution at 75 °C for 2 h and pH value was maintained at 11–12 by adding ammonium hydroxide solution. The completely mixed reactants were suspended for 24 h at room temperature (RT) and then was washed, filtered and dried overnight at 60 °C. The prepared HA nanoparticles were sintered at 1100 °C in order to improve their crystallinity.[36]

FHA preparation

FHA nanoparticles were prepared through sol–gel method in a solution of $Ca(NO_3)_2\cdot 4H_2O$ and $(NH_4)_2HPO_4$ and NH_4F at 75 °C for 2 h and pH value was maintained at 10–11. The definitive reactants were suspended for 72 h at RT, then washed, filtered and repeated the above steps twice and finally dried overnight at 60 °C. The as-prepared FHA nanoparticles were heated at 1100 °C to improve their crystallinity.[37–39]

SiHA preparation

SiHA nanoparticles were prepared *via* sol–gel method in a solution of $Ca(NO_3)_2\cdot 4H_2O$, $(NH_4)_2HPO_4$ and tetraethyl orthosilicate (TEOS) at 75 °C. The pH was also maintained at 10–11 as above. The processes of suspension, lavation and drying were the same with that of HA except that the temperature for sintering SiHA nanoparticles were set at 1200 °C for 2 h.[35]

Characterization and mechanical test

Scanning electron microscopic analysis. Samples' surface morphology was observed under scanning electron microscope (SEM). All powers, previously air dried in RT, were then mounted on aluminum stubs and sputter coated with gold by the Sputter Coater (BIO-RED SC 502; Fisons, Plc, Registered Office, United Kingdom). Finally, the surface morphology and microstructure changes were examined using a SEM (Topcon ABT-60; Japan) and recorded by the analysis 3.0 imaging system (Soft Imaging System; GmbH, Germany).

Transmission electron microscopic analysis. Transmission electron microscope (TEM) (HRTEM, JEOL, JEM-2010FEF, Japan) was used to analyze the crystal structures. Samples were put in 4 mL centrifuge tube filled with ethanol and ultrasonically separated for 15 min to be homogeneously dispersed. Then, the fragments were carefully picked up from the ethanol suspension using a TEM copper mesh coated with carbon film. After drying at RT, samples were directly examined under a TEM at 200 kV.

X-ray photoelectron spectrometer analysis. Quantitative chemical composition was analyzed by an X-ray photoelectron spectrometer (XPS; PHI 5600, multi technique system, Physical Electronics, USA). The XPS spectra was obtained with an Al Kα excitation source (ht1/41486.6 eV) and a take-off angle of 45 at a passing energy of 187.85 eV. All the spectra were obtained after sputtering the coating surface with argon ions to remove possible surface contamination.

X-ray diffraction analysis. X-ray diffraction (XRD) analysis was performed by Rigaku D/MAX 2000 PC X-ray diffractometer (Rigaku, Japan) using CuK radiation at 30 mA and 40 kV. A scanning range from 10 to 80 degrees with a speed of 0.04 degrees per s was used to identify the crystalline phases of the samples. We selected a scanning range from 32.5 to 33.5 degrees at a scanning speed of 0.005 degrees per s for expanded (300) XRD assay.

In vitro cell culture work

Preparation of HA, FHA, SiHA extracts. After sterilization, HA, FHA and SiHA nanoparticles was soaking with α-MEM (α-MEM) (Sigma, USA) at 37 °C for 24 h at the concentration with 625 μg mL^{-1}. The extract was collected by filtrated with 0.22 μm bacterial filter flowing a centrifugation at 1000 rpm for 1 min. Every 40 mL extracts of HA, FHA and SiHA were added with 10% heat-inactivated fetal bovine serum (FBS) (Sigma, USA) and 1% antibiotics (penicillin–streptomycin solution) (P/S; Sigma, USA) respectively. All extracts were used for the following cell culture. And the concentration of F ions of the extract was detected by ion chromatography (IC) (Prodigy 7, LEEMAN LABS Ltd., USA), and Si ions was detected by inductively coupled plasma (ICP) (Optima 4300DV, Perkin Elmer Ltd., USA).

MTT assay. The isolation and culture of bone mesenchymal stem cells (BMSCs) were conducted according to study.[40] The proliferation of BMSCs in material extracts was measured by the MTT assay. In briefly, BMSCs were seeded into 96-well plates at a density of 5×10^3 cells per well. After 24 h of cell adhesion, the culture medium was replaced by 100 μL material extracts medium of HA, FHA, SiHA or blank culture medium per well for 1, 3, 5, 7, 10 days. At each time point, serum free α-MEM with 0.5 mg mL^{-1} MTT (Sigma, USA) was used at 37 °C in 5% CO_2 incubator for 4 h in dark culture. Afterwards, the solution was replaced by dimethylsulfoxide (DMSO) (Sigma, USA) as the

formazan solubilization. The spectrophotometrical absorbance was measured by a microplate reader (BIO-TEK Synergy HT) at wavelengths of 490 nm, with DMSO added non-seeded wells set as blank controls. The optical density (OD) directly showed results.

Fluorescence microscopy analysis. BMSCs were seeded at 5 $\times$ 10^5 cells per well on cell slides in 24-well plate and cultured with HA, FHA and SiHA extracts separately for 1 d, 4 d and 7 d of incubation. Cells were washed with PBS two times and fixed with 4% paraformaldehyde for 15 min at RT. The samples were washed with PBS three times, permeabilized with 0.1% Triton X-100 for 2 min and then washed with PBS two times again. Cells were stained by FITC-phalloidin (5 μg mL^{-1}) for 30 min at RT. After washed with PBS for two times, samples were incubated with DAPI (10 μg mL^{-1}) (Sigma, USA) for 5 min at RT. The stained cells were taken photos by a fluorescent microscopy (Leica, Germany).

Quantitative alkaline phosphatase activity. 3 $\times$ 10^5 BMSCs were seeded in a 24-well plate per well. After cell adherent, culture medium was changed to material extracts containing α-MEM supplemented with 10% FBS, 10 mM sodium β-glycerol phosphate, 50 μg mL^{-1} L^{-1}-ascorbic acids and 1.0 $\times$ 10^{-8} M dexamethasone. Quantitative ALP activity was measured at 7 and 14 days. At each time point, after treated with 200 μL 0.1% Triton X-100 and 2 mM $MgCl_2$ per well to dissolve the cells, then cell suspensions were transferred to 1.5 mL tubes and centrifuged at 14 000 rcf at 4 °C for 10 min. Afterwards, the ALP activity and total amount of protein were determined by *p*-nitrophenyl phosphate method.[41]

Alizarin red staining. The cell seeding density and culture procedures were the same as ALP activity assay. About 0.685 g Alizarin powder was dissolved into 50 mL distilled water, and the staining (pH = 4.2) was adjusted by adding ammonium hydroxide. At day 7 and 14, cells were fixed and stained in Alizarin red solution for 15 min and washed in distilled water to remove excess stain. The calcium nodule staining was photographed by Canon DSLR camera (Nikon Eclipse TS100).

Quantitative real-time RT-PCR. The cell seeding density and culture procedures were the same as in ALP staining. Total RNA was extracted using RNA kit (Omega, USA), reverse transcription was conducted according to the manufacturer's instructions (Takara, Japan). PCR amplification was performed in a real-time PCR system with specific primers for Runx2, OPN and GAPDH. The reaction conditions for PCR were 40 cycles of denaturation at 95 °C for 15 s, annealing at 55 °C for 34 s, and extension at 72 °C for 1 min. Primer sequences for differentiation markers are detailed in Table 1.

Table 1 The Primers used for real-time RT-PCR (GAPDH was used as a housekeeping gene)

Primer	Sequence 5′–3′
OPN	Forward: ACGAATCTCACCATTCCGAT
	Reverse: AGGTCCTCATCTGTGGCATC
Runx2	Forward: ATCCAGCCACCTTCACTTACACC
	Reverse: GGGACCATTGGGAACTGATAGG
GAPDH	Forward: AGAAGGTGGTGAAGCAGGCGG
	Reverse: ATCCTTGCTGGGCTGGGTGG

In vivo study

Femur defect drilling and implantation. All animal procedures were performed in accordance with the Guidelines for Care and Use of Laboratory Animals of Wuhan University, People's Republic of China, and approved by the Ethics Committee at the School of Dentistry (No. 00186867), prior to the start of this experiment. The HA, FHA and SiHA nanoparticles were sterilized before grafting into the femora defects of 6 week-old female SD rats. Six parallel samples were used for each group. A liner skin incision in the distal femoral epimetaphyseal was made bilaterally and blunt dissection of muscles was performed to expose the femoral condyle. A 2.5 mm-diameter latero-lateral bicortical channel was made beneath the growth plate and perpendicular to the shaft axis (Fig. 1). During drilling, sterile saline was used to minimize local heat and to remove debris. The nanoparticles were placed to fill the defects according to group allocation and skin incisions were closed with interrupted sutures. After the operation, all the rats received a subcutaneous injection of penicillin (40 000 IU mL^{-1}) as an antibiotic prophylaxis for three days. Animals were sacrificed randomly at 4 and 8 weeks after material insertion operation, respectively.

μCT analysis. All samples were placed in an embedding mold with 4% paraformaldehyde and scanned by a micro-CT (SkyScan 1172; Bruker-micro CT, Kontich, Belgium) with the X-ray source setting as a voltage of 60 kV and a current of 167 μA using a 0.5 mm aluminum filter. Scans were performed over 360° with a rotation step of 0.7° at a spatial resolution of 15 μm. Then, the scanned data were reconstructed by image analysis software (CT-analyzer; Skyscan). The percent bone volumes (BV/TV), the trabecular thickness (Tb. Th), the bone surface volume ration (BS/BV) and the trabecular separation (Tb. Sp) were measured to analyze the bone regeneration process within the defect.

Histological staining and analysis. After μCT scanning, the harvested samples were decalcified in 10% ethylene diaminetetraacetic acid (EDTA) for eight weeks. The samples were dehydrated in a graded ethanol and embedded in paraffin. Then longitudinal serial sections of 5 μm were cut and mounted on polylysine-coated microscope slides. Each sample was stained with hematoxylin and eosin staining (H&E) and tartrate-resistant acid phosphatase (TRAP) staining (Sigma, USA.). Samples were scanned by Pannoramic MIDI (3D HISTECH, Hungary), and analyzed by Caseviewer.

Antibacterial test. The antibacterial activities were tested against *Porphyromonas gingivalis* (P. g) (ATCC 33277) with the film attachment method which is acknowledged as a popular technique to estimate the antibacterial activity of materials.[42,43]

Bacterial counting on plates. The nanoparticles of three samples were packed into discs with 30 mm in diameter and 2 mm in high with manual hydraulic pump. Each sample group contained 4 plates against bacterial strain for colony counting, the sterilized plates were submerged in sterile saliva at 37 °C for

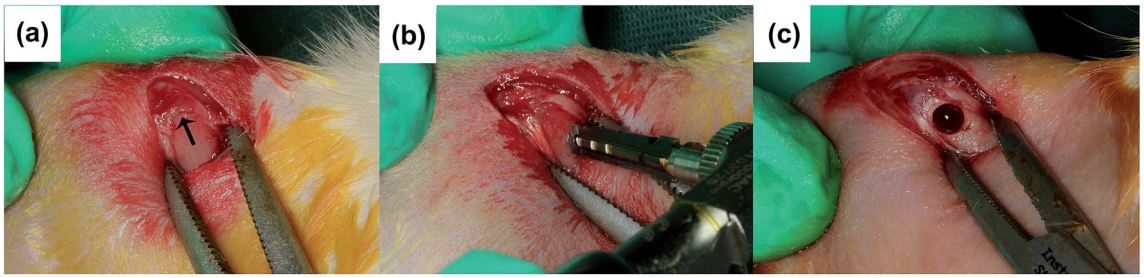

Fig. 1 A 2.5 mm-diameter latero-lateral biocortical channel beneath the growth palate (black arrow) and perpendicular to the shaft axis on rat (a–c).

24 h to form biofilms. A small volume of bacterial suspension (200 μL, 1.0×10^6 CFU mL^{-1}, brain heart infusion (BHI; Bio-Merieux, France)) media with bacteria containing P. g was dropped on a sample surface. After incubation at 37 °C for 48 h under an anaerobic condition (80% N_2, 10% CO_2, and 10% H_2 atmosphere), the samples were separately transferred into a tube containing 10 mL PBS, and vibrated by ultrasonic for 10 min. Then, the bacteria-containing PBS (10 μL) was immediately spread evenly onto a blood agar plate containing BHI supplemented with defibrinated rabbit blood, hemin, and menadione. The BHI blood agar plate was anaerobically incubated at 37 °C for 7 d, and the colony-forming units (CFUs) in the plate were counted by a colony counter (ProtoCOL HR, England).

Live-dead bacterial staining. Every three plates were repeated for live-dead bacterial staining for each group. After culturing bacterial as the above process, the plates were washed by PBS for three times and stained by FITC/PI according Annexin V-FITC Apoptosis detection kit (KeyGEN BioTECH, China). And the samples were observed by an Laser Scanning Confocal Fluorescence Microscope (Olympus FV1000S, Japan).

Statistical analysis. All samples were measured in triplicate. The results were presented as mean ± standard deviation (SD). The data were submitted to analysis of variance, and means were compared by the Student's test. Statistical significance was set to $p < 0.05$.

Result

Characterization of HA, FHA and SiHA

SEM and TEM results illustrated that three kinds of nanoparticles were rod shaped but with different size. HA nanoparticles were 200 nm in length (Fig. 2a and d), while FHA nanoparticles were 700–800 nm in length (Fig. 2b and e) and SiHA nanoparticles were 400–500 nm in length (Fig. 2c and f).

XRD analysis showed typical apatite peaks in all patterns (Fig. 3a–c). The peak intensity of FHA was a little greater than that of HA, and the peak width was a little narrower, indicating better crystallization and higher purity; the peak intensity of SiHA was a little less than that of HA, illustrating weaker crystallization. The results suggested that the adding of F ions in HA would form a more ordered structure with enhanced chemical and thermal stability and adding Si ions in HA nanoparticles was in opposite term.

Fig. 3d–f shows the XPS spectra of HA, FHA and SiHA. For FHA, an F 1s peak was obvious in the wide scan at ~684 eV, which is the fingerprint for fluorine in the FHA structure.[44] An Si 2p peak was evident in the narrow scan at ~102 eV, which is the fingerprint for silicon in the SiHA structure. Moreover, the contents of Ca, F, Si and P in the materials were determined by the ratio of the area under the respective elemental peak in the XPS narrow scan spectrum; the results are presented in Table 2. As demonstrated in Table 2, the measured Ca/P ratios of HA, FHA and SiHA were 1.66, 1.67 and 1.66, respectively; close to the stoichiometric value of 1.67. This indicates that HA with high purity and FHA with a fluoridation degree of 1.1 were formed. The wt% of Si in SiHA was 0.77 wt%, which is close to the theoretical weight of SiHA with 0.8wt% of Si.[45]

The concentration of F ions and Si ions in extracts used in our experiment was illustrated in Table 3. The concentration of F ions in extracts with 625 μg mL^{-1} FHA was 0.3897 mg L^{-1}. And the concentration of Si ions in extract with 625 μg mL^{-1} SiHA was 0.8235 mg L^{-1}.

Cell proliferation

A significant increase in the growth of BMSCs was observed in HA, FHA and SiHA material extracts. All samples showed similar proliferation patterns within 10 days of culture, except for the blank group which had limited proliferation from day 5 ($p < 0.05$) (Fig. 4a and b). Cells in the SiHA group exhibited relatively lower viability than the HA and FHA groups. Interestingly, a similar growth trend was observed in HA, FHA and SiHA group from day 0 to 7. After 7 days, the curve in the FHA group climbed constantly, the proliferation trend in the HA group ceased and even slightly declined ($p > 0.05$).

Cell morphology

Significant differences in the fluorescent microscopy photos were observed among the four groups (Fig. 5). On the one hand, the number of BMSCs in all groups increased over time. On the other hand, the morphology of the BMSCs changed differently during cell spreading and nuclear flattening. On day 1, there were no significant differences in the morphology and number of cells among the groups. On day 4, the number of cells was increased in all groups and the cell density in the SiHA group

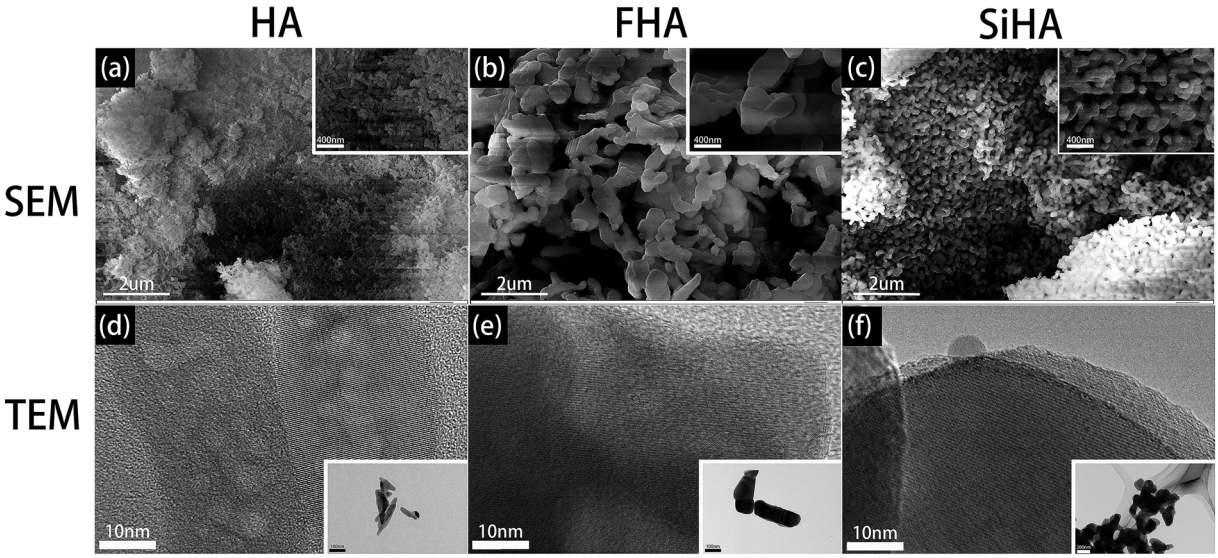

Fig. 2 SEM images of HA (a), FHA (b) and SiHA (c); TEM images of HA (d), FHA (e) and SiHA (f).

was higher than the other three groups. With respect to morphology, there was no obvious changes in the BMSCs in the blank group; BMSCs in this group had spread the most and tended to be spindle shaped and cells in the other three groups presented a clear outline and stereoscopic nucleolus. At day 7, there was a continuous increase in the cell density of all groups;

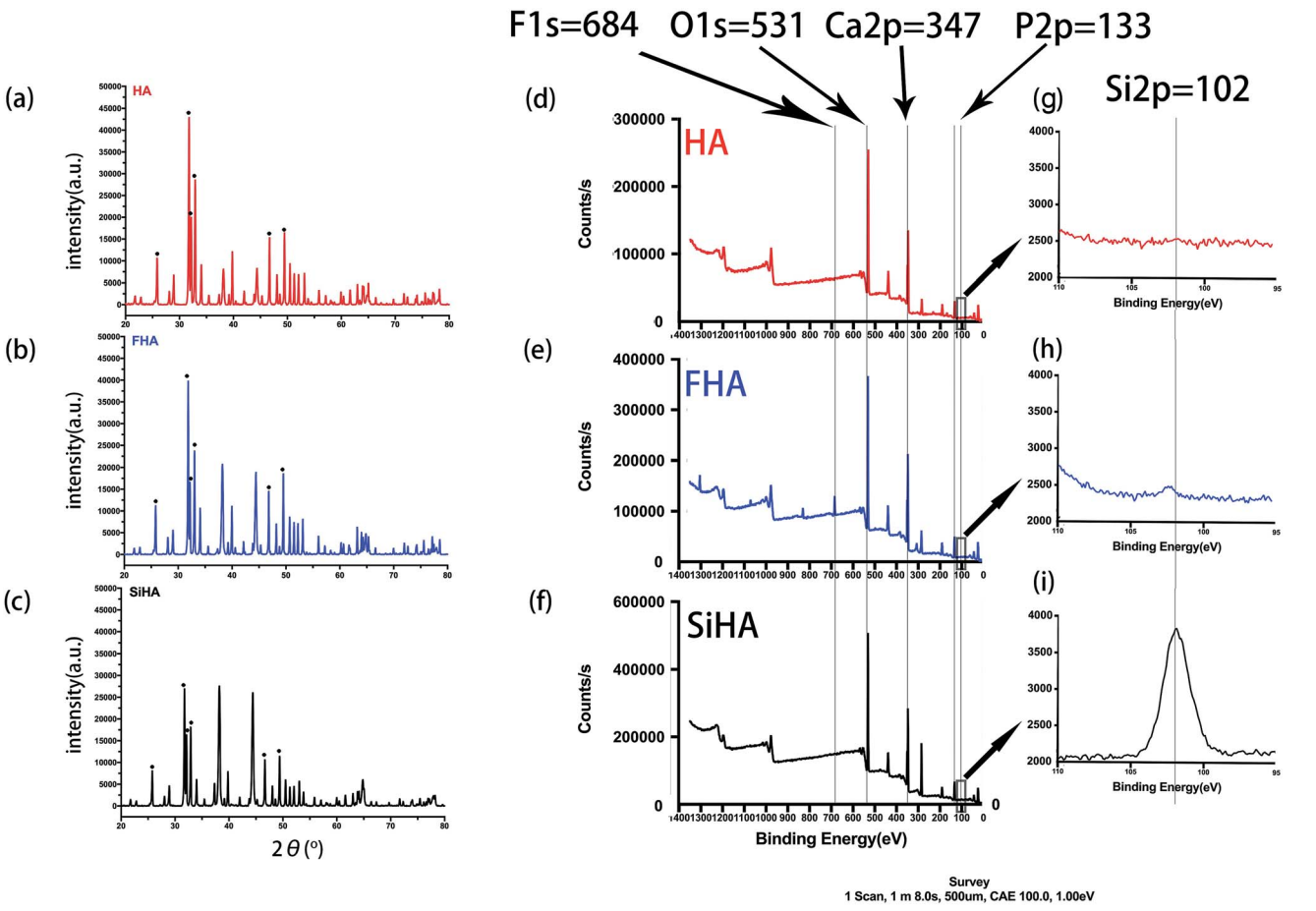

Fig. 3 XRD patterns of sintered HA (a), FHA (b) and SiHA (c) nanoparticles; XPS spectra of HA (d), FHA (e) and SiHA (f); the curve which referred to Si 2p between 105 eV to 110 eV of HA (g), FHA (h) and SiHA (i).

Table 2 Chemical analysis of the samples

Sample	Content atomic%				Atomic ration	Formula
	Ca	P	F	Si	Ca/(P + Si)	
HA	22.18	13.46	—	—	1.66	$Ca_{10}(PO_4)_6(OH)_2$
FHA	21.44	12.84	5.28	—	1.67	$Ca_{10}(PO_4)_6(OH)_{0.9}F_{1.1}$
SiHA	21.12	12.10	—	0.58	1.66	$Ca_{10}(PO_4)_{5.724}(SiO_4)_{0.276}(OH)_2$

Table 3 Ion concentration of sample's extracts

Sample	Ion concentration (mg L^{-1})	
	F	Si
HA	—	—
FHA	0.3897	—
SiHA	—	0.8235

cell density in the SiHA group was still the highest. Cell morphology in the SiHA and HA groups tended to be more elongated, while cells in the FHA group were smaller in size with an irregular shape; these cells appeared to have begun to shrink.

Osteogenic differentiation

Osteogenic differentiation ability was assessed by ALP activity assay and Alizarin red staining. In the ALP activity assay, there were no significant differences in BMSCs on day 7 among all four groups ($p > 0.05$). There were significantly higher levels of ALP activity in the HA, FHA and SiHA groups compared to the blank group ($p < 0.05$) on day 14; there were no significant differences among the HA, FHA and SiHA groups ($p > 0.05$). To further analyse cell mineralization, Alizarin red staining was performed after 7 day and 14 day osteogenic induction (Fig. 6a–h). A few mineralized nodules were formed in the HA, FHA and SiHA groups; no obvious mineralized nodules were noticed in the blank group at day 7. At day 14, obvious mineralized nodules were observed in all groups under a microscope, but the area of mineralization nodules in the FHA group was larger than that of the HA and SiHA groups; the blank group ranked last at the macro level (Fig. 6e–h). The results of Alizarin red staining were in accordance with those of the ALP activity assay.

Runx2 is a key transcription factor that regulates bone development and maintenance of the extracellular matrix,[46] and osteopontin (OPN) is an important marker in the later osteogenic differentiation period. mRNA expression of Runx2 and OPN is shown in Fig. 6j and k, as analysed by quantitative real-time PCR (RT-PCR). Runx2 mRNA expression was highest in the FHA group; there were significant differences between all groups ($p < 0.01$) except for the HA and SiHA groups at day 7 (Fig. 6j). Similar trends in Runx2 mRNA expression were observed at day 14; again, the FHA group exhibited the highest expression. However, mRNA expression of Runx2 increased faster in the SiHA group, resulting in no significant difference between the SiHA and FHA group ($p > 0.05$). OPN mRNA expression in the HA group was significantly higher than the blank group ($p < 0.01$) at day 7. At day 14, the blank group showed the lowest OPN mRNA expression; there were no statistically significant differences among the other three groups. In conclusion, the osteogenic differentiation results above indicate that the ability to promote osteogenesis can be ranked as follows: FHA > SiHA and HA > blank group.

In vivo study

Radiological study. μCT was used to analyse new bone formation at week 4 and week 8 after femur defect surgery and material implantation (Fig. 7). Bone substitutes exhibited high density in 3D reconstruction images (Fig. 7a–h). BV/TV, Tb. Th, BS/BV and Th. Sp were taken as indicators for quantitative analysis (Fig. 7j–l).

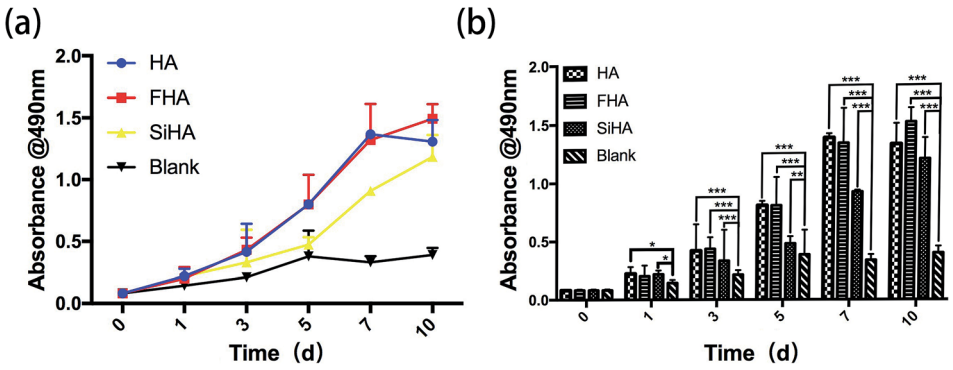

Fig. 4 MTT assay: the cell proliferation image of BMSCs cultured in extracts of HA, FHA, SiHA and α-MEM culture medium from day 1 to day 9 (a and b) ($n = 4$ in each group; $*p < 0.05$).

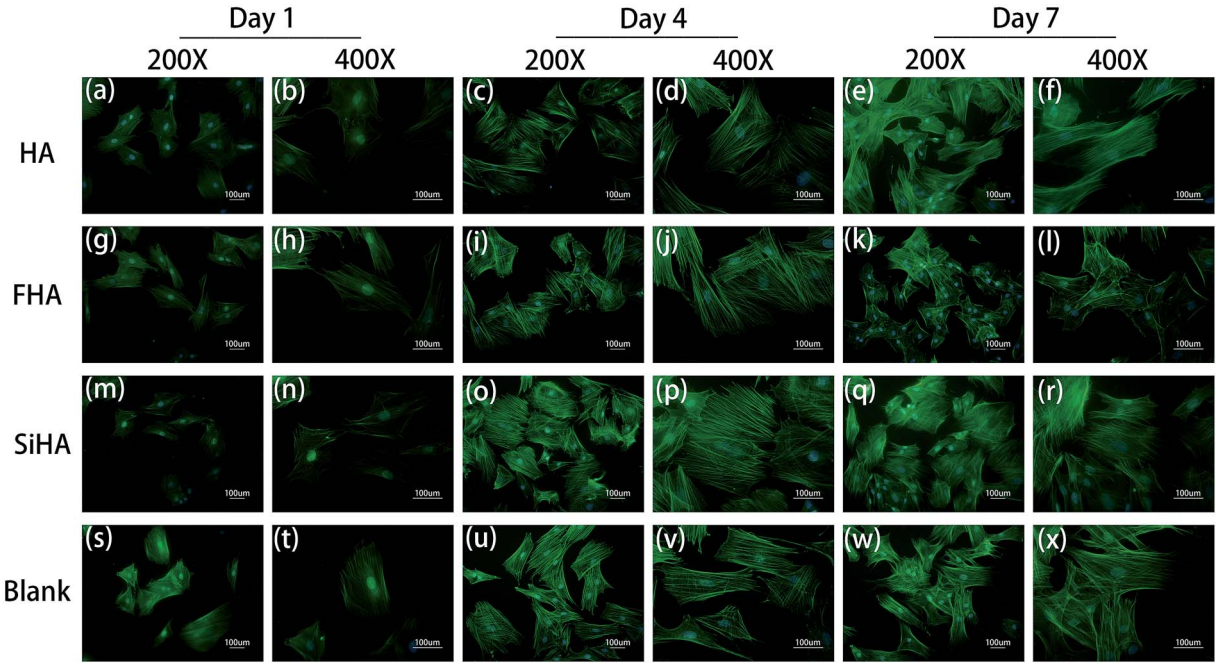

Fig. 5 Cytoskeletal morphology of BMSCs cultured in HA extracts for 1 day (a and b), 4 days (c and d) and 7 days (e and f); cytoskeletal morphology of BMSCs cultured in FHA extracts for 1 day (g and h), 4 days (i and j) and 7 days (k and l); cytoskeletal morphology of BMSCs cultured in SiHA extracts for 1 day (m and n), 4 days (o and p) and 7 days (q and r); cytoskeletal morphology of BMSCs cultured in α-MEM culture medium for 1 day (s and t), 4 days (u and v) and 7 days (w and x).

At week 4, the SiHA group exhibited the highest BV/TV and Tb. Th ($p < 0.05$), followed by the FHA and HA groups. There was no statistically significant difference in the BV/TV value between the FHA and HA groups, but the FHA group exhibited a better Tb. Th value than the HA group. The BS/BV value was ranked as follows: SiHA < FHA < HA < blank group ($p < 0.05$). The SiHA group exhibited the lowest Th. Sp value, but there were no statistically significant differences between the other three groups. At week 8, the BV/TV and Tb. Th values of the SiHA group were still the highest. BV/TV in the FHA group increased obviously and was significantly higher than the HA group ($p < 0.05$). The BS/BV value exhibited the opposite trend to the BV/TV value. For the Th. Sp value, all three bone substitute groups occupied a smaller space compared to the blank group ($p < 0.05$).

Histological evaluation. Histological evaluation was performed by haematoxylin-eosin (H&E) staining on the distal femoral metaphysis defect sites 8 weeks after implantation (Fig. 8A–D and a–d). A 1 cm-diameter boundary could still be observed in all groups owing to the bone defect drilling surgery; immature and irregular new bone was filled in the bone defect areas; and there was still an amount of material remnants surrounded by immature new bone in the material-implanted groups (Fig. 8A–D). The morphology and bone trabecular orientation tended to be distinct in each group. The trabecula space in the HA group was smaller than the other groups, while the blank group exhibited the largest newly-formed trabecula space (Fig. 8a–d).

TRAP staining was used to study osteoclastic activity with osteoclasts in brownish-red staining. Most of the stained cells were distributed around the pore space and close to the material remnants; these had not degraded at that time point. The greatest number of stained osteoclasts were observed in the HA group (Fig. 8e) followed by the SiHA group (Fig. 8g). Less osteoclasts were observed in the other two groups (Fig. 8f and h).

Antibacterial activity. Fig. 9a–c shows the agar media with P. g which was pre-cultured in HA, FHA or SiHA leaching liquor for 48 hours. Comparison of the bacterial CFUs on the HA, FHA and SiHA specimens revealed differences in antibacterial activity. Histograms (Fig. 9d) provide quantitative comparisons between the CFU numbers. The FHA group exhibited the highest antibacterial activity against P. g relative to the other two nanoparticle plates ($p < 0.01$).

The viability of P. g on the three plates was also determined by fluorescence staining, as shown in Fig. 9e–m. After bacterial invasion for 48 hours, there were large amounts of viable bacteria (green fluorescence) on the HA plates and SiHA plates, and only small amounts of dead bacteria (red fluorescence) could be observed on the SiHA plates. In comparison, the amounts of living and dead bacteria on the FHA plates were both smaller than the other two kinds of nanoparticles.

Discussion

Bone defects remain a challenge due to limitations associated with the sources of autogenous bone grafts. A good bone substitute must possess several properties such as biocompatibility, bioactivity, osteoconduction, osteoinduction, non-toxicity, *etc.*[47] To better understand the application of HA, FHA and SiHA nanoparticles, we compared the osteoclastic activity, antibacterial abilities and the *in vitro* and *in vivo* osteogenesis of the three materials. We fabricated HA, FHA and

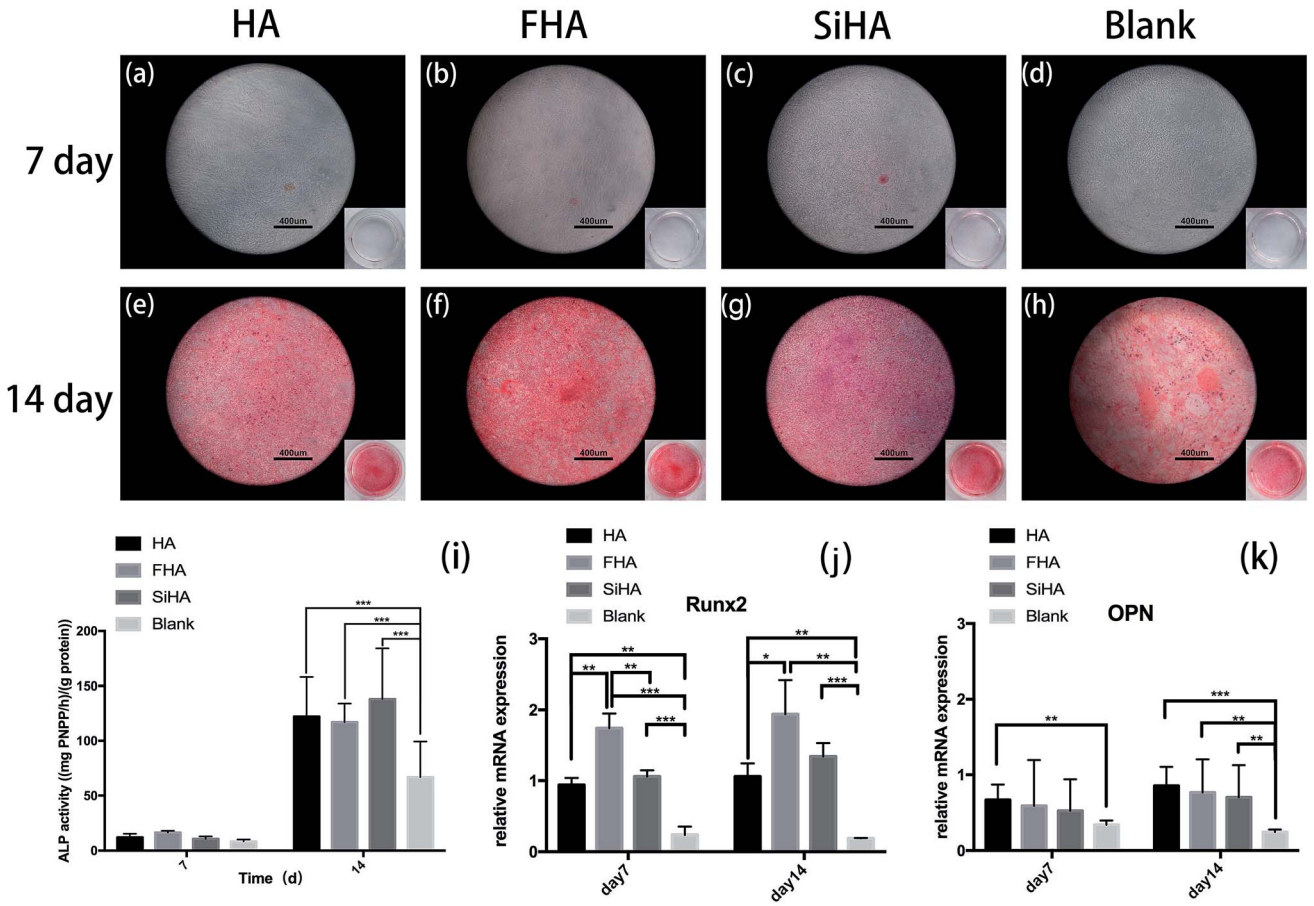

Fig. 6 Alizarin red staining of BMSCs cultured in HA, FHA, SiHA extracts and α-MEM culture medium under osteogenic induction for 7 days (a–d) and 14 days (e–h). Quantitative ALP activity of BMSCs cultured in HA, FHA, SiHA and α-MEM culture medium with mineralized solution for 7 days and 14 days (i) ($n = 4$ in each group; $*p < 0.05$). Real-time PCR analysis of mRNA Runx2 and OPN in BMSCs cultured in HA, FHA, SiHA extracts and α-MEM culture medium under osteogenic induction for 7 days (j) and 14 days (k) ($n = 4$ per group; $*p < 0.05$).

SiHA using the sol–gel method,[48] and analysed by SEM, TEM, XRD and XPS assay. The SEM results showed that all three nanoparticles had rod-like particles with approximate lengths of 200 nm, 700 nm and 450 nm for HA, FHA and SiHA, respectively. According to previous studies, we fabricated HA and FHA nanoparticles with molar Ca/P ratios approaching a value of 1.67 and SiHA nanoparticles with a molar Ca/(P + Si) ratio approaching 1.67. Further, FHA with a fluoridation degree of 1.1 was formed. The wt% of Si in SiHA was 0.77 wt%, which is close to the theoretical weight of SiHA with 0.8 wt%.[34,45] And the concentration of F ions in extract with FHA was 0.3897 mg L^{-1}, which is accordance to the proper level (ranging from 0.1 to 100 μM) and can promote proliferation and differentiation of BMSCs.[14,21] And the concentration of Si ions in extract with SiHA was 0.8235 mg L^{-1}, which is also at a proper level (under 5 mM) to promote BMSCs.[49]

These characteristics indicate the successful fabrication of the three kinds of nanoparticles.

Many studies have reported that HA,[4–6] FHA[14–17] and SiHA[32] possess the potential to promote cell proliferation and differentiation. In this study, cell proliferation potential was in accordance with former studies and the *in vitro* osteogenic enhancing capability of the three nanoparticles was ranked as follows: FHA > SiHA > HA; SiHA nanoparticles demonstrated the best osteogenic capability *in vivo*.

HA has received substantial research attention as a classic bone substitute that can accelerate bone formation *via* increasing cell proliferation and differentiation. The literature suggests that nanoparticles 100–250 nm in diameter have better repairing ability.[50] The mechanism mainly can be summarized as follows. First, HA influences the metabolism of osteoblasts. When HA nanoparticles are absorbed in bone tissue, the released Ca and P ions promote ALP activity and stimulate bone formation.[51] Second, HA takes parts in bone vascularization, which is key in the process of bone repair.[52] HA can enhance cell responsiveness to vascular endothelial growth factor (VEGF) *via* NOS activity, causing microvascular endothelium to differentiate into capillary-like structures[53] quickly.

With regard to FHA, F ion doping is an effective way to improve the biological properties of HA. Fluoride at a proper concentration, ranging from 0.1 to 100 μM, can significantly enhance both osteoblast proliferation and differentiation.[14,21,54,55] The mechanism by which fluoride promotes cell proliferation and osteoblast activity is highly complicated and has not yet been clearly clarified. Studies suggest that fluoride promotes osteoblast proliferation by enhancing the effect of growth factor-

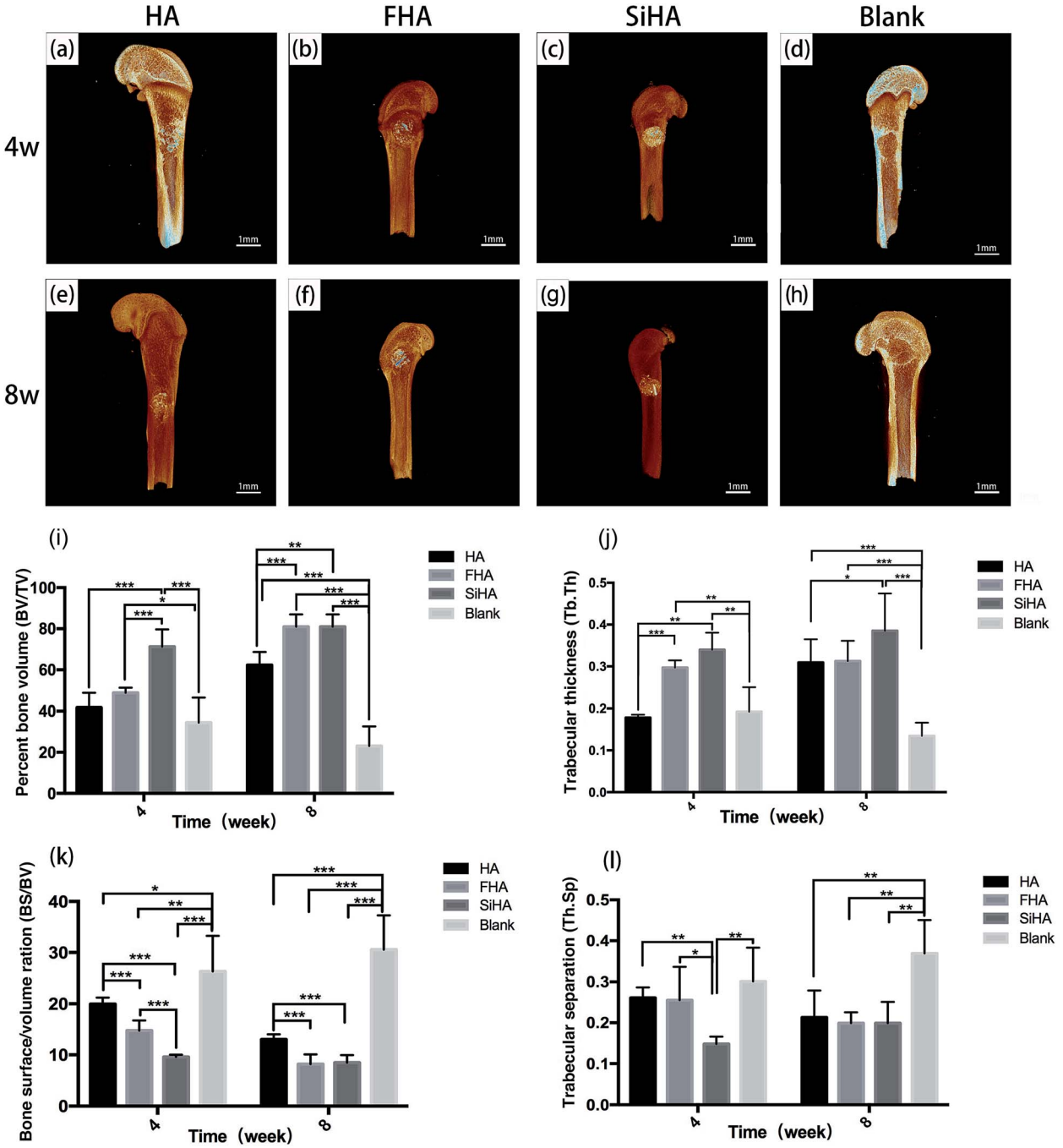

Fig. 7 3D reconstruction μCT images of the femurs defects filled with HA (a and e), FHA (b and f), SiHA (c and g) and blank (d and h) 4 weeks and 8 weeks after surgery. Percent bone volume analysis (BV/TV) (i), trabecular thickness (Tb. Th) (j), bone surface/volume ration (BS/TV) (k) and trabecular separation (Tb. Ts) (l) of new bone formation in the defect areas filled with HA, FHA, SiHA for 4 weeks and 8 weeks ($n = 4$ per group; $*p < 0.05$).

mediated stimulation of the Ras-Raf-MAPK mitogenic signal transduction pathway.[19,20] Another study suggested that fluoride may influence the Wnt/β-catenin signalling pathway in osteoblasts, which is known to play an important role in regulating cell proliferation, differentiation and morphogenesis.[56,57] Fluoride was reported to induce the phosphorylation of Akt at serine 473 and subsequently activate the phosphorylation of glycogen synthase kinase-3β (GSK-3β) at serine 9, leading to inhibition of GSK-3β activity and activation of Wnt/β-catenin signalling.[21] However, it has been shown that small doses of F ions can promote the proliferation and differentiation of osteoblasts[7,58] while large doses of F ions can inhibit osteoblast proliferation and differentiation and induce cell apoptosis[58] because of cell metabolism imbalance.[17] In this study, although FHA was found to promote cell proliferation, the cell morphology revealed that cells in FHA group at day 7 showed shrinking morphology may be related to the accumulation of F ions (Fig. 5k and l).

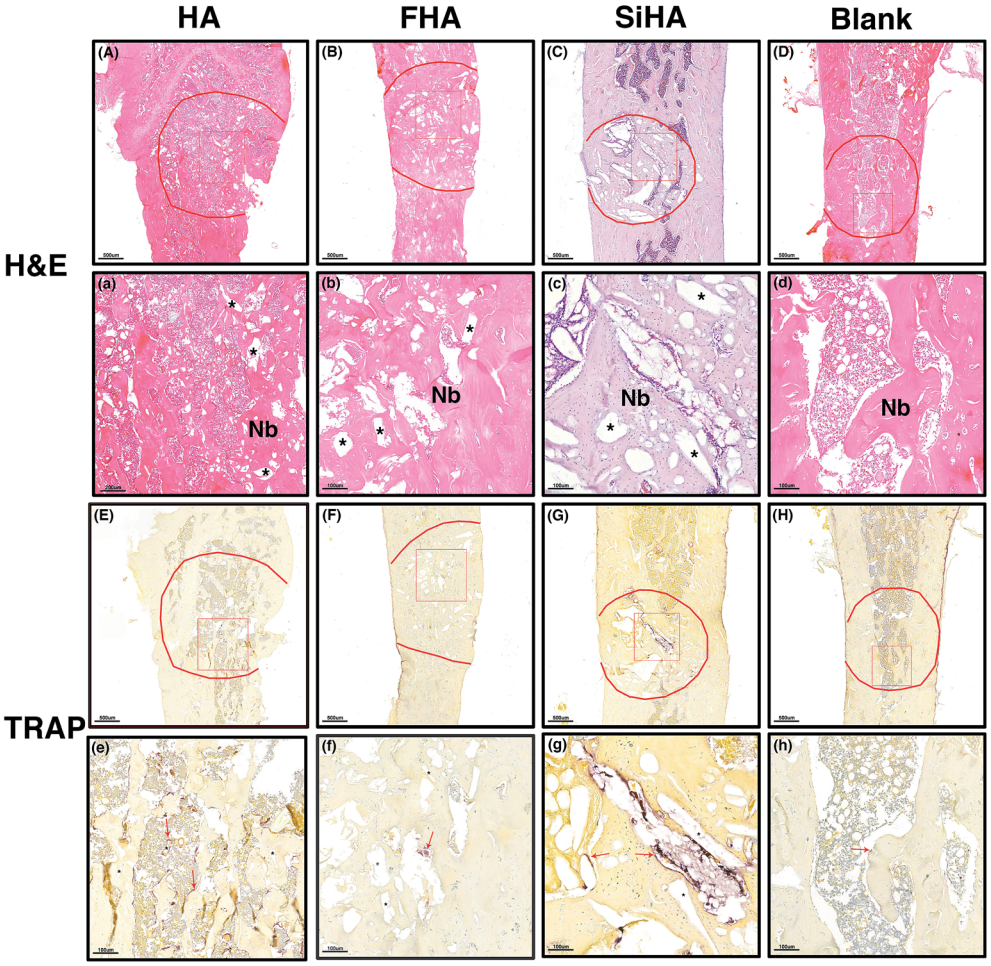

Fig. 8 Hematoxylin- and eosin-stained histological morphology of the bone defects 8 weeks after filled with, HA (A and a), FHA (B and, b), SiHA (C and c) and blank (D and d). New bone (Nb) formation observed in all groups and the pore space (*) around Nb was no degraded material of HA, FHA, and SiHA. Trap staining of osteoclasts (red arrow) was observed around HA (E and e), FHA (F and f), SiHA (G and g) and blank (H and h), scale bar is 500 μm (A–H) and 100 μm (a–h).

Si ion doping is another important way to modify the biological properties of HA nanoparticles. Si ions can stimulate collagen type I synthesis and osteoblastic differentiation both *in vivo* and *in vitro*.[59,60] Research has revealed that Si ions can activate the MAPK-ERK pathway in osteoblast-like cells[61] and Si ions can enhance cellular differentiation and collagen production *via* the TGF-β pathway by the binding of TGF-β1 to its cognate receptors.[62] Further, Si ions can significantly upregulate AXIN2, β-catenin, SHH and patched-1 (PTCH1) gene expression.[49] AXIN2 and β-catenin are a critical members of the Wnt/β-catenin signalling pathway;[63–65] SHH is one of the ligands of the Hedgehog-Gli signalling pathway and PTCH1 is a target gene of the SHH-Gli signalling pathway.[66] All of these signalling pathways are involved in cell proliferation and differentiation.[56,57,67–69] Beyond that, orthosilicic acid (SiO_4^{4-}), which exists in SiHA, could regulate the expression of miR-146a to suppress the activity of NF-κB; this would influence both osteoblast differentiation and activity.[70–73] It should be noted that when the concentration of Si ions is higher than 5 mM, which is much larger than that of FHA (0.1 to 100 μM), it may suppress cell proliferation. This could be due to the cytotoxicity of high concentrations of Si ions or the change in the pH and extracellular ionic environment.[49]

Bone formation and resorption appears to be a dynamic process. Aside from osteoblasts, osteoclasts are also involved in bone regeneration, especially during the degradation of materials.[74–76] With regard to FHA, fluoride with concentration lower than 8 mg L^{-1} will decrease the activity of new formed osteoclasts because but will not affect osteoclasts formation, involving in inhibiting NFATc1 and downstream functional genes, such as DC-STAMP, c-Src, Atp6v0d2, MMP9, and CK; this leads to impaired capacity for osteoclast acidification and reduced secretion of proteolytic enzymes.[77] When the concentration of F ions is between 0.5–1.0 mM, the number of resorption lacunae made by individual osteoclasts and the resorbed area per osteoclast is decreased.[78] The pH value is also important for osteoclasts. Osteoclasts can be activated with pH values from 6.7 to 7.0,[79] but the activity of osteoclasts is suppressed when pH > 7.0.[80] The releasing F ion will increase the pH, resulting in less activity of osteoclasts. According to our results in Fig. 8E–H and e–h, the number of osteoclasts in the FHA group was significantly less than the other two groups.

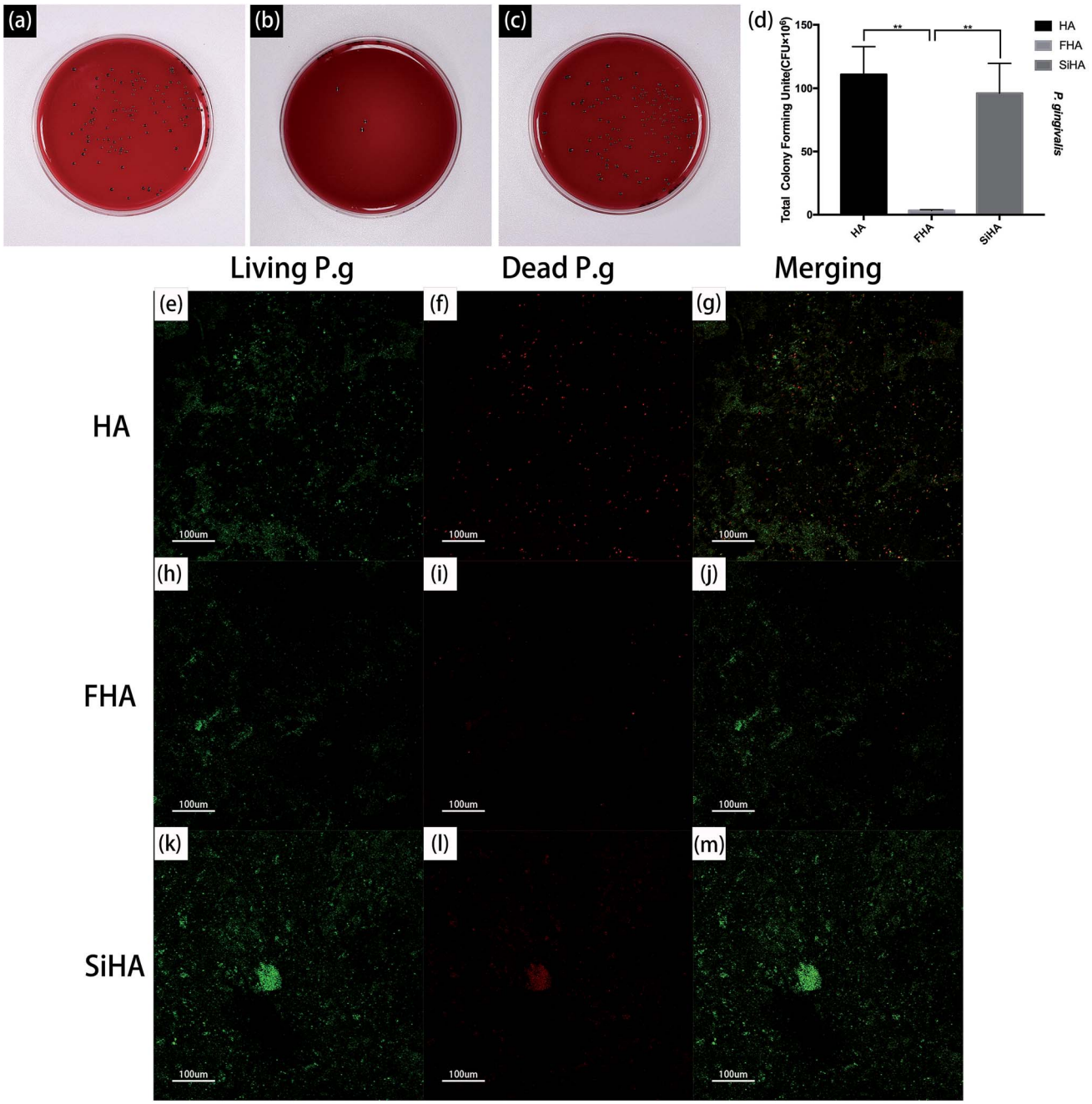

Fig. 9 Photographs of Columbia blood agar media with colonies of P. g strains after incubation with HA (a), FHA (b) and SiHA (c) respectively and statistical results corresponding to the survivability of bacteria on three types of sample surfaces (d) $n = 3$ per group; $*p < 0.05$). Fluorescence microscopy images showing viability of the adherent *P. gingivalis* on the plates of three specimens respectively, as displayed by SYTO® 9 and PI dyes. HA (e, f and g), FHA (h, i and j) and SiHA plates (k, l and m).

Several studies have reported that Si can also inhibit the activity of osteoclasts. Osteoprotegerin (OPG)/receptor activator for nuclear factor-κB ligand (RANKL) ratio plays a critical role in pre-osteoclast maturation and osteoclast activation. In normal physiological conditions, RANKL combines with receptor activator for nuclear factor-κB (RANK) which distributes on the surface of pre-osteoclast to promote the differentiation and activation of osteoclasts. Silica stimulates OPG transcription with unchanged RANKL;[81,82] thus, OPG competes with RANKL to bind to (pre)osteoclastic receptor RANK, negatively affecting pre-osteoclast maturation and osteoclast activation.[82,83] Accordingly, the SiHA group exhibited less osteoclasts in TRAP staining compared to the HA group, but more osteoclasts than the FHA group (Fig. 8).

It is important for bone substitutes to possess good osteogenic potential, but it is also important to prevent infection in the bacteria-filled microenvironment. Many studies have illustrated that fluoride can prevent dental caries. Further, fluoride can also inhibit pathogenesis in periodontal disease. P. g, a Gram-negative anaerobic bacterium implicated as a major pathogen associated with peri-

implantitis and periodontitis,[84] was used in this experiment to evaluate the antibacterial ability. The results demonstrated that P. g was obviously inhibited on FHA plates compared to the other two materials. The contact angle of FHA will increased along with the amount of F ions adding; this is associated with increased hydrophobicity, which reduces the initial adhesion of bacteria.[85] Further, F ion released from FHA acts in several ways to affect bacteria metabolism. For instance, it can act as an inhibitor of the glycolytic enzyme, enolase.[85] Further, fluoride complexes are responsible for fluoride-induced inhibition of proton translocating F-ATPases by mimicking phosphate to form complexes with ADP at the reaction centres of enzymes. ATPase plays an important role in the maintenance of intracellular pH by pumping out protons; inhibition of this enzyme disrupts bacterial metabolism and aciduric capability.[86,87] Beyond that, fluoride ions inhibit acid-producing bacteria like *Fusobacterium nucleatum* (F. n) and *Treponemas*, which are periodontal pathogens; this helps to maintain a normal acid–base balance necessary for proper osteogenesis. Fluoride ions are released when bacterial metabolism begins and pH diminishes. The release of F ions can inhibit bacteria growth, stabilize the microenvironment and resistant the inflammatory process.[88]

Conclusion

HA, FHA and SiHA nanoparticles could promote osteogenesis and FHA and SiHA did better than HA. FHA and SiHA could both promote BMSCs proliferation, but FHA showed a better performance in osteogenesis *in vitro*, while SiHA did better *in vivo*. FHA suppressed osteoclasts activity and presented significant antibacterial properties. In conclusion, FHA and SiHA both can be a potential bone substitutes. However, FHA might be an ideal material in bone regeneration especially in infectious bone defects.

Conflicts of interest

There are no conflicts to declare.

Acknowledgements

This project was supported by the Fundamental Research Funds for the Central University of China (No. 2042018kf0108).

Notes and references

1 J. Van der Stok, E. M. M. Van Lieshout, Y. El-Massoudi, G. H. Van Kralingen and P. Patka, *Acta Biomater.*, 2011, **7**, 739–750.
2 S. V. Dorozhkin and M. Epple, *Angew. Chem., Int. Ed. Engl.*, 2002, **33**, 3130–3146.
3 S. F. Hulbert, F. A. Young, R. S. Mathews, J. J. Klawitter, C. D. Talbert and F. H. Stelling, *J. Biomed. Mater. Res.*, 1970, **4**, 433–456.
4 W. Suchanek and M. Yoshimura, *J. Mater. Res.*, 1998, **13**, 94–117.
5 D. W. Hutmacher, J. T. Schantz, C. X. F. Lam, K. C. Tan and T. C. Lim, *J. Tissue Eng. Regener. Med.*, 2007, **1**, 245–260.
6 A. S. Brydone, D. Meek and S. Maclaine, *Proc. Inst. Mech. Eng., Part H*, 2010, **224**, 1329–1343.
7 Y. Wang, S. Zhang, X. Zeng, L. L. Ma, W. Weng, W. Yan and M. Qian, *Acta Biomater.*, 2007, **3**, 191–197.
8 T. S. B. Narasaraju and D. E. Phebe, *J. Mater. Sci.*, 1996, **31**, 1–21.
9 G. L. Darimont, B. Gilbert and R. Cloots, *Mater. Lett.*, 2004, **58**, 71–73.
10 S. Overgaard, M. Lind, K. Josephsen, A. B. Maunsbach, C. Bünger and K. Søballe, *J. Biomed. Mater. Res.*, 1998, **39**, 141.
11 I. Baltag, K. Watanabe, H. Kusakari, N. Taguchi, O. Miyakawa, M. Kobayashi and N. Ito, *J. Biomed. Mater. Res., Part B*, 2000, **53**, 76.
12 M. Šupová, *Ceram. Int.*, 2015, **41**, 9203–9231.
13 G. Graziani, M. Bianchi, E. Sassoni, A. Russo and M. Marcacci, *Mater. Sci. Eng., C*, 2016, **74**, 219–229.
14 J. R. Farley, J. E. Wergedal and D. J. Baylink, *Science*, 1983, **222**, 330.
15 M. Kassem, L. Mosekilde and E. F. Eriksen, *Eur. J. Endocrinol.*, 1994, **130**, 381–386.
16 B. Y. Reed, J. E. Zerwekh, P. P. Antich and C. Y. Pak, *J. Bone Miner. Res.*, 1993, **8**, 19.
17 D. Burgener, J. P. Bonjour and C. P. D. Joseph, *J. Bone Miner. Res.*, 1995, **10**, 164–171.
18 K. A. Bhadang and K. A. Gross, *Biomaterials*, 2004, **25**, 4935–4945.
19 K.-H. W. Lau and D. J. Baylink, *J. Bone Miner. Res.*, 1998, **13**, 1660–1667.
20 K.-H. W. Lau and D. J. Baylink, *J. Bone Miner. Res.*, 2003, **18**, 1897–1900.
21 L. Pan, X. Shi, S. Liu, X. Guo, M. Zhao, R. Cai and G. Sun, *Toxicol. Lett.*, 2014, **225**, 34–42.
22 R. E. Marquis, *Can. J. Microbiol.*, 1995, **41**, 955–964.
23 H.-W. Kim, Y.-M. Kong, Y.-H. Koh, H.-E. Kim, H.-M. Kim and J. S. Ko, *J. Am. Ceram. Soc.*, 2003, **86**, 2019–2026.
24 M. Okazaki and R. Z. Legeros, *Adv. Dent. Res.*, 1996, **10**, 252.
25 H. W. Kim, H. E. Kim and J. C. Knowles, *Biomaterials*, 2004, **25**, 3351.
26 H. W. Kim, Y. M. Kong, C. J. Bae, Y. J. Noh and H. E. Kim, *Biomaterials*, 2004, **25**, 2919.
27 E. M. Carlisle, *Science*, 1970, **167**, 279–280.
28 E. M. Carlisle, *Science*, 1972, **178**, 619–621.
29 E. M. Carlisle, *J. Nutr.*, 1980, **110**, 1046–1056.
30 M. López-Álvarez, E. L. Solla, P. González, J. Serra, B. León, A. P. Marques and R. L. Reis, *J. Mater. Sci.: Mater. Med.*, 2009, **20**, 1131.
31 S. R. K. Meka, S. Kumar Verma, V. Agarwal and K. Chatterjee, *ChemistrySelect*, 2018, **3**, 3762–3773.
32 N. Patel, S. M. Best, W. Bonfield, I. R. Gibson, K. A. Hing, E. Damien and P. A. Revell, *J. Mater. Sci.: Mater. Med.*, 2002, **13**, 1199–1206.
33 S. R. K. Meka, V. Agarwal and K. Chatterjee, *Mater. Sci. Eng., C*, 2019, **94**, 565–579.
34 K. A. Hing, P. A. Revell, N. Smith and T. Buckland, *Biomaterials*, 2006, **27**, 5014–5026.

35 M. Honda, K. Kikushima, Y. Kawanobe, T. Konishi, M. Mizumoto and M. Aizawa, *J. Mater. Sci.: Mater. Med.*, 2012, **23**, 2923–2932.
36 L. Yubao, J. D. Wijn, C. P. A. T. Klein, S. V. D. Meer and K. D. Groot, *J. Mater. Sci.: Mater. Med.*, 1994, **5**, 252–255.
37 Y. Chen and X. Miao, *Biomaterials*, 2005, **26**, 1205–1210.
38 G. Penel, G. Leroy, C. Rey, B. Sombret, J. P. Huvenne and E. Bres, *J. Mater. Sci.: Mater. Med.*, 1997, **8**, 271.
39 L. M. Rodríguez-Lorenzo, J. N. Hart and K. A. Gross, *Biomaterials*, 2003, **24**, 3777–3785.
40 N. O. Grad, P. Emoke and I. A. Mironiuc, *Clujul Med.*, 2014, **86**, 65–68.
41 C. Wu, R. Miron, A. Sculean, S. Kaskel, T. Doert, R. Schulze and Y. Zhang, *Biomaterials*, 2011, **32**, 7068–7078.
42 H. Jing, Z. Yu and L. Li, *J. Biomed. Mater. Res., Part A*, 2008, **87**, 33–37.
43 W. K. Son, J. H. Youk, T. S. Lee and W. H. Park, *Macromol. Rapid Commun.*, 2004, **25**, 1632–1637.
44 M. A. Stranick and M. J. Root, *Colloids Surf.*, 1991, **55**, 137–147.
45 A. Aminian, M. Solati-Hashjin, A. Samadikuchaksaraei, F. Bakhshi, F. Gorjipour, A. Farzadi, F. Moztarzadeh and M. Schmücker, *Ceram. Int.*, 2011, **37**, 1219–1229.
46 J. H. Jonason, G. Xiao, M. Zhang, L. Xing and D. Chen, *J. Dent. Res.*, 2009, **88**, 693–703.
47 G. Aaron and P. P. Weitzel, *Sports Med. Arthrosc. Rev.*, 2007, **15**, 158.
48 M. Esnaashary, M. Fathi and M. Ahmadian, *Int. J. Appl. Ceram. Technol.*, 2014, **11**, 47–56.
49 P. Han, C. Wu and X. Yin, *Biomater. Sci.*, 2013, **1**, 379–392.
50 W. Zhu, J. Xiao, D. Wang, J. Liu, J. Xiong, L. Liu, X. Zhang and Y. Zeng, *Int. Orthop.*, 2009, **33**, 567–571.
51 B. Chang-Jun, K. Hae-Won, K. Young-Hag and K. Hyoun-Ee, *J. Mater. Sci.: Mater. Med.*, 2006, **17**, 517–521.
52 K. Woo Seob and K. H. Koo, *J. Korean Med. Sci.*, 2005, **20**, 479–482.
53 S. Pezzatini, L. Morbidelli, R. Solito, E. Paccagnini, E. Boanini, A. Bigi and M. Ziche, *Bone*, 2007, **41**, 523–534.
54 J. E. Wergedal, K. H. Lau and D. J. Baylink, *Clin. Orthop. Relat. Res.*, 1988, **233**, 274–282.
55 W. J. Qu, D. B. Zhong, P. F. Wu, J. F. Wang and H. Bo, *J. Bone Miner. Metab.*, 2008, **26**, 328–334.
56 Y. Huang, X. Jin, X. Zhang, H. Sun, J. Tu and T. Tang, *Biomaterials*, 2009, **30**, 5041–5048.
57 B. Zhang and J. Ma, *Protein Cell*, 2010, **1**, 898–906.
58 C. Y. C. Pak, J. E. Zerwekh and P. Antich, *Trends Endocrinol. Metab.*, 1995, **6**, 229–234.
59 F. H. Nielsen and R. Poellot, *J. Trace Elem. Exp. Med.*, 2004, **17**, 137–149.
60 D. M. Reffitt, N. Ogston, R. Jugdaohsingh, H. F. Cheung, B. A. Evans, R. P. Thompson, J. J. Powell and G. N. Hampson, *Int. Rev. Gesamten Hydrobiol. Hydrogr.*, 2003, **70**, 27–46.
61 M. Y. Shie, S. J. Ding and H. C. Chang, *Acta Biomater.*, 2011, **7**, 2604–2614.
62 J. Li, L. Wei, J. Sun and G. Guan, *J. Biomater. Appl.*, 2013, **27**, 595–604.
63 Y. Hsiao-Man Ivy, J. Boris, S. Tzong-Jen, L. Bo, C. Frank, P. J Edward, B. Walter and H. Wei, *Development*, 2005, **132**, 1995.
64 E.-h. Jho, T. Zhang, C. Domon, C.-K. Joo, J.-N. Freund and F. Costantini, *Mol. Cell. Biol.*, 2002, **22**, 1172–1183.
65 N. Barker, *Methods Mol. Biol.*, 2008, **468**, 5.
66 M. Varjosalo and J. Taipale, *Genes Dev.*, 2008, **22**, 2454–2472.
67 P. N. De Aza, Z. B. Luklinska, A. Martinez, M. R. Anseau, F. Guitian and S. De Aza, *J. Microsc.*, 2000, **197**, 60–67.
68 T. Yusuke, I. Satoshi, A. V. Kaneshiro, E. Shigeyuki, J. E. Frencken and F. R. Tay, *Dent. Mater.*, 2006, **22**, 647–652.
69 S. V. Prykhozhij, *PLoS One*, 2010, **5**, e13549.
70 J. Chang, Z. Wang, E. Tang, Z. Fan, L. Mccauley, R. Franceschi, K. Guan, P. H. Krebsbach and C. Y. Wang, *Nat. Med.*, 2009, **15**, 682–689.
71 Y. Masato, F. Hidefumi, S. Masashi, K. Takenobu, D. Takahiro, T. Tetsu and J. Eijiro, *J. Biol. Chem.*, 2009, **284**, 35987.
72 L. Yan, L. Aimin, S. Karen, Z. Hongying, M. S. Nanes and W. M Neale, *J. Bone Miner. Res.*, 2007, **22**, 646–655.
73 X. Zhou, F. M. Moussa, S. Mankoci, P. Ustriyana, N. Zhang, S. Abdelmagid, J. Molenda, W. L. Murphy, F. F. Safadi and N. Sahai, *Acta Biomater.*, 2016, **39**, 192–202.
74 K. Dennis, S. K. Wasim, H. Behrooz and M. David, *Curr. Stem Cell Res. Ther.*, 2013, **8**, 185–191.
75 Z. Gu, W. Hao, L. Li, Q. Wang and X. Yu, *Biomed. Mater.*, 2012, **7**, 065007.
76 S. Wenisch, J.-P. Stahl, U. Horas, C. Heiss, O. Kilian, K. Trinkaus, A. Hild and R. Schnettler, *J. Biomed. Mater. Res., Part A*, 2003, **67**, 713–718.
77 J. Pei, B. Li, Y. Gao, Y. Wei, L. Zhou, H. Yao, J. Wang and D. Sun, *Environ. Toxicol.*, 2014, **29**, 588–595.
78 A. Okuda, J. Kanehisa and J. N. M. Heersche, *J. Bone Miner. Res.*, 1990, **5**, S115–S120.
79 I. R. Orriss and T. R. Arnett, *Methods Mol. Biol.*, 2012, **816**, 103–117.
80 T. R. Arnett and D. W. Dempster, *Endocrinology*, 1986, **119**, 119–124.
81 F. Maehira, Y. Iinuma, Y. Eguchi, I. Miyagi and S. Teruya, *J. Bone Miner. Metab.*, 2008, **26**, 446.
82 M. Wiens, X. Wang, H. C. Schröder, U. Kolb, U. Schloßmacher, H. Ushijima and W. E. G. Müller, *Biomaterials*, 2010, **31**, 7716–7725.
83 H. C. Schröder, X. H. Wang, M. Wiens, B. Diehl-Seifert, K. Kropf, U. Schloßmacher and W. E. Müller, *J. Cell. Biochem.*, 2012, **113**, 3197–3206.
84 S. S. Socransky and A. D. Haffajee, *J. Periodontol.*, 1992, **63**, 322–331.
85 Nurhaerani, K. Arita, Y. Shinonaga and M. Nishino, *Dent. Mater. J.*, 2006, **25**, 684.
86 M. Yoshinari, Y. Oda, T. Kato and K. Okuda, *Biomaterials*, 2001, **22**, 2043.
87 M. F. Hayacibara, O. P. Rosa, H. Koo, S. A. Torres, B. Costa and J. A. Cury, *J. Dent. Res.*, 2003, **82**, 267–271.
88 W. D. Nordquist, O. Hajima, K. Yutaka, K. Kazunari, O. Toshimitsu and D. J. Krutchkoff, *J. Oral Implantol.*, 2011, **37**, 35–42.

